DYNAMIC APERTURE STUDIES FOR THE FCC-ee*

L. Medina[†], Universidad de Guanajuato, Leon, Mexico
R. Martin, Humboldt-Universität zu Berlin, Germany
R. Tomas, F. Zimmermann, CERN, Geneva, Switzerland

Abstract

Dynamic aperture (DA) studies have been conducted on the latest *Future Circular Collider – ee* (FCC-ee) lattices as a function of momentum deviation. Two different schemes for the interaction region are used, which are connected to the main arcs: the crab waist approach, developed by BINP, and an update to the CERN design where the use of crab cavities is envisioned. The results presented show an improvement in the performance of both designs.

INTRODUCTION

The FCC-ee is a proposed high luminosity e^+e^- collider [1,2] with a center-of-mass energy from 90 to 350 GeV. The ring has separate beam pipes for electrons and positrons, which intersect at two or four interaction points (IPs). The FCC-ee is a potential intermediate step in a global study towards a 100 TeV hadron collider –the FCC-hh– sharing the same 100 km tunnel. A first parameter set, used as a basis for the design study, has been published [3]. One of the main constraints of the FCC-ee design is the imposed limit of 50 MW of synchrotron radiation per beam. Four operation energies have been proposed, with beam energies of 45 , 80 , 120 , and 175 GeV, corresponding to the Z pole, the WW threshold, the HZ cross-section maximum, and the top pair threshold, respectively.

The present DA studies have been performed for the lattice at a beam energy of 175 GeV, for which the off-momentum DA is most critical.

Table 1: Lattices Under Study

Opt.	Ring	Interaction Region	Comments
1	R-v14	CW-v13	Crab off
2	R-v14	CW-v14	Crab off, set 1
3	R-v14	CW-v14	Crab off, set 2
4	R-v14	CW-v14	Crab on, set 2
5	R-v16	CW-v14	Crab off, set 2
6	R-v16	Small crossing angle	Crab cavity

LATTICES

Six main lattices, called options 1 to 6 in Table 1, have been studied. In our model, the main arc is enclosed by the left and right sides of the interaction region (IR), with the interaction point located at their respective ends; the complete ring is a sequence of four of this structures (i.e. 4 IPs). Each of the main arcs is composed of three arcs
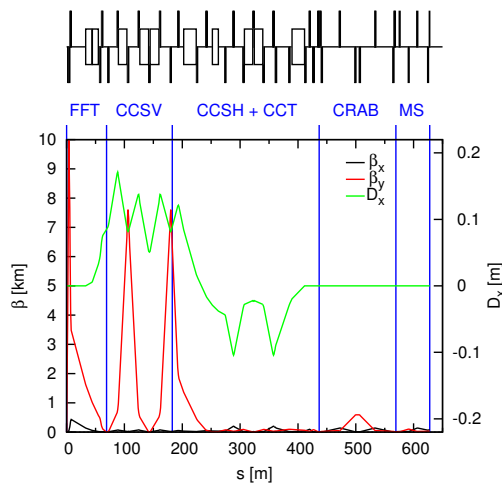
(a) Crab waist scheme.
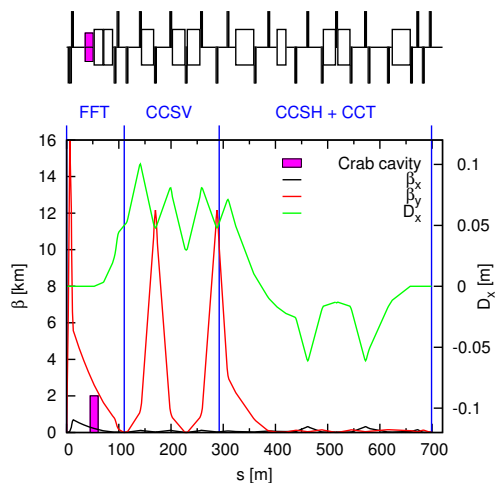
(b) Small crossing angle scheme.

Figure 1: General layout and optical functions of the IR.

and two RF cavity sections. Ring versions 14 (R-v14) and 16 (R-v16) differ in the structure of the basic arc cell, the number and position of the arc sextupoles, and the horizontal phase advance attained, namely 90° for R-v14, and 79.2° for R-v16 [4]. A set of quadrupole strengths for the basic arc cells of R-v16 with 90° phase advance is also available, but this configuration has not been explored.

The first design for the IR follows a crab waist (CW) scheme [5,6]; the advantage of such approach is the higher luminosity at the lower beam energies. Its general layout and beta functions are shown in Fig. 1a, and consists of a final telescope (FFT), dedicated chromaticity correction sections for both transverse planes (CCSV and CCSH), a chromaticity correction telescope (CCT) that also provides

the last bending to the arc, a crab waist (CRAB), and a matching section (MS). The sextupoles in the CRAB section are off for most part of this study, with the exception of option 4, where the integrated strength [7] is given by

$$K = \frac{1}{2\theta_c} \frac{1}{\beta_y^* \beta_y} \sqrt{\frac{\beta_x^*}{\beta_x}}, \qquad (1)$$

where θ_c is the crossing angle, and $\beta_{x,y}$ and $\beta_{x,y}^*$ are the beta functions at the sextupole and the IP, respectively. Crab waist sextupoles on the left and right sides of the IR have opposite polarity, and their phase advances with respect to the IP meet the following conditions:

$$\Delta\mu_x = m\pi, \qquad \Delta\mu_y = \tfrac{1}{2}(2n+1)\pi,$$

where m and n are positive integers. Crab waist version 13 (CW-v13) contains an achromatic bend between the CRAB and MS sections, which has been eliminated in version 14. CW-v14 was tested for two sets of sextupole strengths, delivering two different momentum acceptances. For the second set –the one that delivers the largest momentum acceptance–, the effect of the sextupole at the crab waist was studied. The distance between the beams at the end of the IR has been significantly reduced in CW-v14.

The design of the alternative IR concept was obtained by removing the last two sections from CW-v14, and scaling it by a factor of 1.6. By doing so, the total length extends to 700 m, which corresponds to the baseline of the FCC-hh IR [8]. Fig. 1b shows the corresponding β functions and the position of the crab cavity to be studied in the future as means to attain higher luminosities. The total crossing angle $2\theta_c$ has been reduced from 30 to 11 mrad. This design is an attempt to overcome the limitations of the previous small crossing angle lattices [9, 10], as well as to reduce the high synchrotron radiation power produced in the BINP layout due to stronger dipole magnets.

Syncrotron Radiation

Synchrotron radiation going into the detector region is reduced by a factor of ~12 in the small crossing angle scheme, compared to the CW scheme (Table 2). This is due to the lengthening of the lattice and the reduction of the bending angles to keep the geometry. By doing so, however, the needed dispersion for the chromaticity correction is reduced as well. Since the chromaticity correction requirements determine the sextupole strengths, their values will increase, degrading the DA.

Momentum Acceptance

The momentum acceptance has been calculated for each of the aforementioned lattices. The variation of the non-

Table 2: Synchrotron Radiation into Detector Region [11]

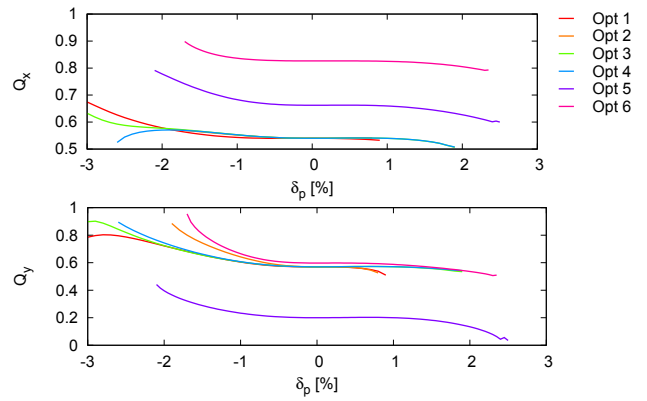|	Crab waist	Small cross. ang.
Power	2.6 MW	193 kW

Figure 2: Horizontal and vertical momentum acceptance.

integer part of the horizontal and vertical tunes Q_x and Q_y as a function of the relative momentum deviation $\delta_p = \Delta p/p$ is shown in Fig 2. The extent of the curves represents the existence of a stable orbit. The evolution of the CW design is followed by an increase in momentum acceptance, and in its latest option, the range is centered around $\delta_p = 0\%$. The small crossing angle scheme has a momentum acceptance similar to the latter, but with a slight reduction on range.

DYNAMIC APERTURE STUDIES

The DA for each lattice has been calculated by particle tracking using MAD-X and PTC. The number of turns in the simulations varies between 200 and 800, which correspond to almost 9 and 35 times the longitudinal damping time. The simulations do not take into account fringe-field effects, synchrotron motion or synchrotron radiation. For the small crossing angle IR, the effect of the cavity itself is not taken into account either. The DA at the IP is presented in units of the beam size, whose values are listed in Table 3 for both schemes. By running the tracking simulation for different momentum deviations spanning the full momentum acceptance, it is possible to determine the minimum DA as a function of δ_p for each lattice.

RESULTS

Several comparisons can been performed between the six options under study, as is shown in Fig. 3.

In Fig. 3a, we see a consistent stability region in options 1 to 3 for the on-momentum case, keeping the same magnitude on the horizontal axis for all of them, but increasing for the second and third options in the vertical plane. Thus, for particles with $\delta_p = 0\%$, the change from CW-v13 to CW-v14

Table 3: Optical Properties at the IP for Both IR Schemes

Parameter	Unit	Crab waist	Small cross. ang.
β_x^*/β_y^*	m/mm	0.5/1.0	1.28/1.27
$\epsilon_x^*/\epsilon_y^*$	nm/pm	2.13/4.25	2.0/2.0
σ_x^*/σ_y^*	μm/nm	0.326/0.652	0.506/0.503

(a) Effect of the change of IR from CW-v13 to CW-v14, crab off.

(b) Effect of the crab sextupoles in the crab waist IR.

(c) Effect of the change phase advance in the arc cells.

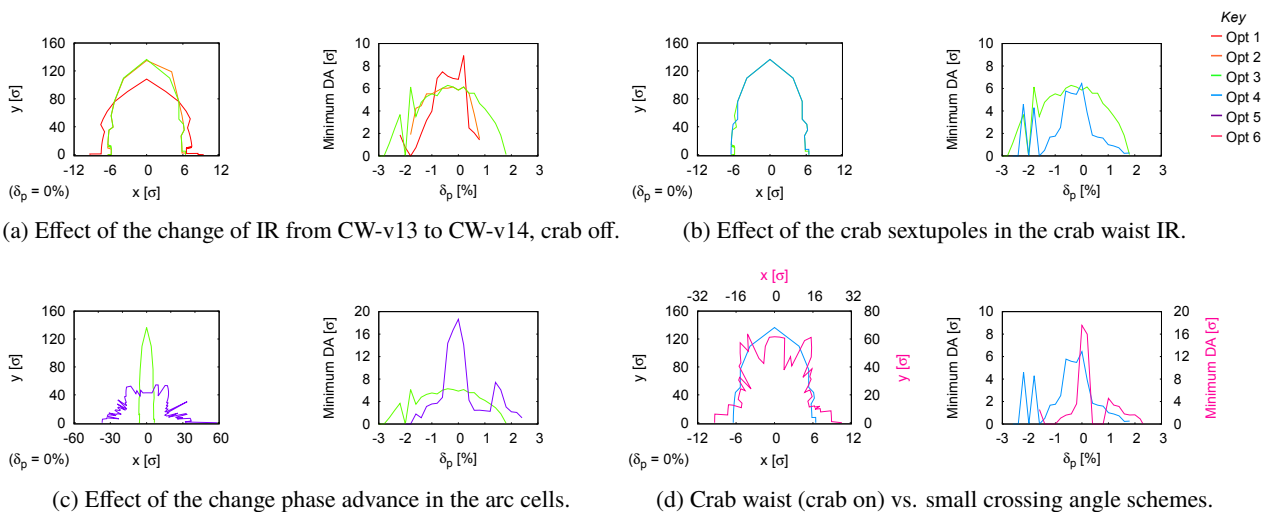(d) Crab waist (crab on) vs. small crossing angle schemes.

Figure 3: Comparison between the results of the six options listed in Table 1. For each item, the left plot shows the DA for $\delta_p = 0\%$ and the right corresponds to the minimum DA, for the options involved *(key)*. Secondary axes apply to option 6.

improves the vertical aperture and does not have a considerable impact horizontally. Although the minimum DA for the first option is around 1σ larger than the corresponding value in the other two options, it decreases more rapidly for off-momentum particles compared to the second and third options. Sets 1 and 2 change the momentum acceptance, as previously mentioned, but do not have a significant impact in terms of on-momentum DA. Both options 2 and 3 have their highest minimum DA at $\delta_p = 0\%$, and decrease smoothly to zero for larger values of momentum deviation. Therefore, option 3 is the best not only thanks to the larger momentum acceptance, but also in view of its overall behaviour.

Figure 3b shows the comparison between options 3 and 4, that is, between lattices with crab sextupoles off and on (Eq. 1), respectively. Although the effect crab sextupoles is negligible for the on-momentum case, a strong dependence of the minimum DA with δ_p is evident. DA goes to zero around $\delta_p \approx -2.0\%$ in all lattices following the CW scheme.

Going away from the 90° phase advance in the basic arc cells significantly improves the on-momentum DA, as shown in Fig. 3c. The stability region for on-momentum particles has drastically changed: although the vertical amplitude has decreased to less than a half of the corresponding value in the previous options, the DA along the horizontal axis has increased considerably (going even beyond 60σ for positive values). Option 5 addresses the optimization suggested in [12], which consists in setting the working point (Q_x, Q_y) away from resonance conditions by choosing an appropriate phase advance per cell in the arcs. However, such optimization only applies to on-momentum particles, delivering lower values for particles with large momentum deviations than for option 3 (except by an increase around +1.4%). A more general approach for DA improvements is required then.

Figure 3d presents a comparison between the small crossing angle scheme and the latest IR following the CW approach (crab on). Since option 6 has different optical proper-

ties at the IP according to Table 3, the results are displayed in terms of the corresponding beam size (secondary axes). On-momentum DA for the small crossing angle design is roughly 24σ and 20σ horizontally (positive and negative), and 60σ vertically. The horizontal DA values in the small crossing angle IR are greatly increased compared to their counterparts in the CW scheme with sextupoles on. The opposite situation occurs in the vertical plane, where the DA has decreased.

CONCLUSION

The design of an interaction region for the FCC-ee with an momentum acceptance of around 2% and broad DA in that range, is a very challenging task. The off-momentum DA is considerably reduced by crab sextupoles, and the change in horizontal phase advance of the arc cells to 79.2° only improves the on-momentum results.

The small crossing angle scheme inherits the momentum acceptance and DA properties of the CW design on which it is based, while delivering weaker magnets that significantly reduce the synchrotron radiation power going into the detector region. In both schemes, the off-momentum DA remains very small for a feasible IR design.

The small crossing angle scheme is currently at an early stage and there is a lot of potential optimization still to be done. For instance, a refined matching between the IR and the arc optics –with special attention paid to the Montague W functions–, the choice of an appropriate working point, the shortening of L^* to reduce the chromaticity, and the correction of higher order chromaticities, may improve the properties of both approaches.

REFERENCES

[1] The FCC-ee Design Study website: `tlep.web.cern.ch`

[2] M. Koratzinos, "FCC-ee Accelerator Parameters, Performance and Limitations", *arXiv: 1411.2819* (2014).

[3] J. Wenninger et al., "Future Circular Collider Study Lepton Collider Parameters", *CERN EDMS No. 1346082* (2014).

[4] B. Harer, "Status of the Lattice Design and the Chromaticity Correction Scheme in the Arcs", FCC-ee Accelerator VIDYO meeting No. 14 (2015). `https://indico.cern.ch/event/373936/`

[5] A. Bogomyagkov et al., "Beam-Beam Effects Investigation and Parameters Optimization for a Circular e^+e^- Collider at Very High Energies", *Phys. Rev. ST Accel. Beams* 17, 041004, 2014.

[6] A. Bogomyagkov et al., "Interaction Region of the Future Circular Electron-Positron Collider FCC-ee", TUPTY018. *These proceedings*, Richmond, VA, USA (2015).

[7] P. Raimondi et al., "Beam-Beam Issues for Colliding Schemes with Large Piwinski Angle and Crabbed Waist", *LNF-07/001 (P)* (2007).

[8] A. Ball et al., "Future Circular Collider Study Hadron Collider Parameters", *CERN EDMS No. 1342402* (2014).

[9] H. Garcia et al., "FCC-ee Final Focus with Chromaticity Correction", THPRI010, *Proceedings of IPAC'14*, Dresden, Germany (2014).

[10] R. Martin et al., "Status of the FCC-ee Interaction Region Design", *CERN-ACC-2015-25* (2015).

[11] H. Burkhardt et al., "Tools for Flexible Optimization of IR Designs with Application to FCC", TUPTY031. *These proceedings*, Richmond, VA, USA (2015).

[12] P. Piminov, "Nonlinear Dynamic Study of FCC-ee", FCC-ee Accelerator VIDYO meeting No. 13 (2015). `https://indico.cern.ch/event/367430/`